BS 2019 2-4 SEPT ROME 16th IBPSA INTERNATIONAL CONFERENCE AND EXHIBITION

INTERNATIONAL BUILDING PERFORMANCE SIMULATION ASSOCIATION

Numerical Analysis and Evaluation of Large-Scale Hot Water Tanks and Pits in District Heating Systems

Abdulrahman Dahash, Michele Bianchi Janetti and Fabian Ochs
Unit of Energy Efficient Buildings, Department of Structural Engineering and Material Sciences, University of Innsbruck, Innsbruck, Austria

Abstract

A key lever to overcome the challenges in buildings sector related to today's extensive utilization of fossils (e.g. global warming) is to integrate renewables (e.g. solar energy) into district heating systems. However, solar energy fluctuates based on seasonal and hourly patterns. This pinpoints the significance of seasonal thermal energy storage (STES) systems. This work investigates the numerical modeling of two STES (tank and pit). Since the groundwater existence can reduce the STES performance and, on the other hand, the STES has an influence on the groundwater, the paper examines the performance of an underground tank with existence of groundwater.

Introduction

District heating (DH) is often envisioned as a key option for efficient heat-supply in urbans and cities (Dahash, A. et al., 2019). Yet, the existing DH infrastructure is mostly fossils based, which contributes to the production of pollutant emissions. Therefore, there is a high desire to integrate renewables (RE) in this energy scheme in order to mitigate the emissions, maintain higher primary energy savings and lower the DH temperature resulting into a more sustainable system.

Out of renewables, solar energy is often considered the most dominant source. As a result, research has been ongoing to address the exploitation of solar energy in heat-supply applications (e.g. DH systems) in order to reduce the deployment of fossils. In the recent years, the number of solar district heating (SDH) systems have been growing and its scale varies from small-scale systems (i.e. neighborhoods) to large-scale systems (e.g. cities) (Mazhar, A. R. et al., 2018). It is held that this type of DH assists in the transition from our current energy scheme to more sustainable scheme.

Solar energy, however, fluctuates seasonally and daily as it is the case with most of RE. For instance, higher solar energy yield is observed in the summer season, whereas the higher heating demand (e.g. space heating and domestic hot water in residential applications) is noted in winter during which very low outdoor temperature are recorded (Allegrini, J. et al., 2015). Thus, one of the main challenges impeding the full transition to SDH systems is the intermittency in solar energy. Consequently, thermal energy storage systems found a prominent role in solar thermal applications since it bridges the gap between the solar availability in summer and the winter heating demand.

Thermal energy storage (TES) is often underlined not only as a mature technology that addresses the redundancy of a RE-based energy system, but also as a key player in the transition phase to RE (Dahash, A. et al., 2019). The goal of this large-scale technology is to store the solar heat captured in summer and use it later in winter when heat is demanded. Thereby, large-scale TES systems contribute significantly to the improvement of penetration of RE share and abatement of emissions (Dahash, A. et al., 2019).

TES systems are not only limited to renewables-based applications. In contrast, they are also commonly deployed for combined heat and power (CHP) applications in order to smooth the operation and to provide higher flexibility.

Large-scale TES systems require large available areas and they store energy for long timescales and, accordingly, the most promising types of seasonal thermal energy storage (STES) are placed satisfactorily under the ground, where the temperature varies less than that in the ambient. The most common types of STES are tank thermal energy storage (TTES), pit thermal energy storage (PTES), aquifer thermal energy storage (ATES) and borehole thermal energy storage (BTES) (Ochs F. , 2009).

TES losses, in particular those of STES, are function of several parameters: storage temperature, storage surface area, storage time, storage type and thermal properties of the surroundings (especially the case of a soil with groundwater flow) (Dahash, A. et al., 2018).

Further, thermal losses might have an impact on the ground/soil exposing them to an increase in the temperature. Thereby, the groundwater temperature gradually increases violating some given hydro-geological standards (i.e. maximum of 20°C to 25°C) as it is the case in some countries. Consequently, it is important to locate the STES properly, where no influence (or minimal influence) is realized on the groundwater or to minimize the losses.

Hence, STES design process (pre-design, design, planning, evaluation and optimization phases) is an interrelated complex process due to a wide list of variables (e.g. location, hydrogeological conditions, construction type, size, geometry, materials and storage medium) (Dahash, A. et al., 2019). Down to these actors, real experimental investigations on STES is frequently

https://doi.org/10.26868/25222708.2019.210566

held to be challenging because the investment cost can be enormous with a performance below expectations. Hence, STES and system simulations are perfectly suited to examine the large-scale systems (Ochs F. , 2014).

In this paper, the authors firstly present the development of numerical models for two options of large-scale TES (i.e. tank and pit) for SDH applications. Then, the work underlines the applicability of 2-D and 3-D multiphysics numerical models. To test the models, the work examines the impact of groundwater flow on the storage performance. Finally, the work investigates the functionality of cut-off walls whether they are capable of minimizing thermal losses in order to preserve a high performance of the storage systems and to reduce the impact on the groundwater temperature.

Previous STES Modeling Studies

STES numerical modeling arise as an alternative approach to real experimental investigations. Thereby, it is allowable to examine the influence of any boundary condition on the STES performance without any actual economical cost. However, it is often held that numerical STES models tend to be costly in terms of simulation time. Despite the fact that STES research has received a great attention in literature, it is challenging to address multi-tasking STES models with low computation costs.

As an example, Panthalookaran et al. reported numerical CFD models that are ideally suited for specific tasks (i.e. charging/discharging modes) (Panthalookaran, V. et al., 2008). The models were validated against measured data from two buried storage tanks in Germany. One of the tanks is installed in Hannover–Kronsberg with a volume of 2750 m^3, whilst the other is the underground TES in Friedrichshafen–Wiggenhausen with a volume of ca. 12,000 m^3. The models were used to develop a new characterization method for performance evaluation of various boundary designs during standby mode in large-scale stratified TES (Panthalookaran, V. et al., 2011).

CFD simulations require large computation efforts and, presently, this is often seen not practical as well in the near future. Consequently, assumptions are frequently set for a number of inputs (e.g. material properties and boundary conditions) in simulation. These assumptions produce, in fact, a positive notable reduction in the computation efforts forming the so-called “coarse models” (Ochs F. , 2009). For instance, Ochs presented a dynamic numerical model based on finite element discretization (Ochs F. , 2014). The model was able to represent various TES shapes (cylinder, cone) for underground hot water TES in Matlab/Simulink platform. Then, the model was further coupled to a finite difference model for the ground.

Moving to TRNSYS, there exist two coarse models; the XST model (type 342) that simulates buried cylindrical water tanks. The other is the ICEPIT-model (type 343), which represents buried gravel-water pits. The ICEPIT-model outperforms XST-model because it simulates several shapes (i.e. cylindrical tanks and truncated cones), whilst the XST-model simulates only cylindrical geometries (Dahash, A. et al., 2019).

In coarse models, the “notable” reduction has a cost that often results into a shortcoming in the depiction of thermal hydraulic behavior in STES. Thus, coarse models do not accurately account for thermal losses, especially when the case comes to a more complicated modeling scheme (e.g. presence of groundwater flow).

Moving to a comparison between design and actual results, Schmidt and Sørensen recently published monitoring results from some large-scale STES in Denmark (Schmidt, T. and Sørensen, P. A., 2018). They found that the storage efficiency of, for example, Marstal pit heat storage for 2015 was around 62 % a bit higher than the design value of 61 %. Moreover, Chang et al. investigated the influences of the key characteristic parameters on the thermal performance of PTES using a CFD code validated with experimental data from in-situ test rig with a lab-scale (Chang, C. et al., 2017).

In this work, the authors firstly present 2-D axial symmetrical models that are able to represent STES systems with circular cross sections (i.e. tanks and conical pits) and its surroundings. Then, the same approach is used to develop 3-D models that account for groundwater flow.

Methodology

Development of numerical modeling

At this level, two STES numerical models are developed using the numerical modeling tool COMSOL Multiphysics© 5,4. Because both tank and conical pit are axially symmetrical, this implies that it is enough to model a single half of the storage.

Furthermore, COMSOL Multiphysics offers a 2-D axisymmetric modeling environment with cylindrical coordinate system for such geometries, therefore; both STES models are implemented by taking advantage of these features.

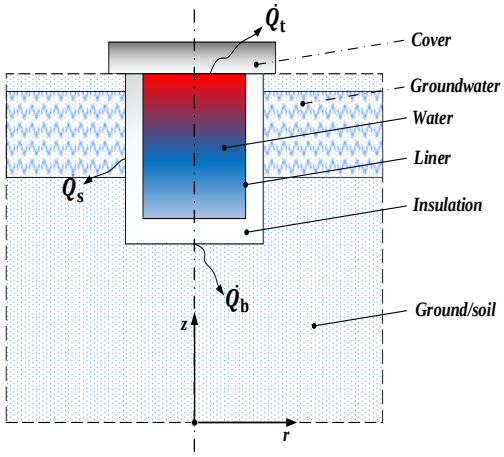

Figure 1: A 2-D representation of an underground tank with groundwater.

Governing equations

In the 2-D STES model, the mass of the water flowing in/out the STES is held conserved and, accordingly, the steady-state continuity equation for the water is given as follows:

$$\dot{m}_{\text{in}} = \dot{m}_{\text{out}} = \dot{m} = \rho \cdot \dot{V}_{\text{w}} \quad (1)$$

Whereas the energy stored in a one of the central volume elements can be described by the following equation:

$$\begin{aligned}(\rho A c_p)\frac{\partial T(t)}{\partial t} = &-(\rho c_p \dot{V}_{\text{w}})\nabla T + A\nabla\cdot(\lambda_{\text{w}}\nabla T)\\ &- U_{\text{wall}}\cdot(\pi d)\cdot(T(t)\\ &- T_{\text{ground}}(t))\end{aligned} \quad (2)$$

Where ρ, c_p, $\dot{m}$ and $\dot{V}_{\text{w}}$ represent the density, specific heat capacity, mass and volumetric flowrates of the fluid, respectively. Where U_{wall} stands for the thermal transmittance of the storage envelope (fluid to ground), whereas A is the cross-section area of the layer. Moreover, when the simulation reaches the upper layer (1st layer); another heat loss term ($\dot{Q}_{\text{t}}$) is accounted for and, therefore, A_{top} is used to include the upper surface area of the first segment in calculations. The same applies when the calculation reaches the last layer in the storage model; thereby, the heat loss from the bottom ($\dot{Q}_{\text{b}}$) is included.

A buoyancy driven heat flow is often observed during the standby mode often known as (storage phase or cooling mode). This heat flow results from buoyancy inducing a natural convection process, which causes a recirculation of water between the hot and cold areas. In order to include this effect in equation (2), the water conductive term ($A\nabla\cdot(\lambda_{\text{w}}\nabla T)$) is replaced by another term to enhance the thermal conductivity of water and, consequently, to exclude inverse thermocline. Thus:

$$= \begin{cases} A\nabla\cdot(\lambda_{\text{w}}\nabla T) & , \quad \dot{V}_{\text{w}} \neq 0 \\ A\nabla\cdot(\lambda_{\text{w,enh}}\nabla T), & \dot{V}_{\text{w}} = 0 \; and \; \dfrac{\partial T}{\partial z} < 0 \end{cases} \quad (3)$$

Further, the heat transfer also occurs in the ground and it is described by the following equations:

$$(\rho_{\text{g}} c_{p,\text{g}})\frac{\partial T_{\text{g}}(t)}{\partial t} = \nabla\cdot\dot{q} \quad (4)$$

One major shortage of axisymmetric models is the challenge to include the unsymmetrical flow of groundwater, which will eventually violate the symmetry constraints. Hence, 3-D numerical models arise as a quintessential option. Nevertheless, 3-D models usually possess more degrees of freedom due to extra mesh elements and, thus, more simulation time.

Similar to the 2-D model, the fluid domain in the STES is represented by equations (1-3). In addition, the heat transfer in the ground layers, through which no groundwater flows, are described by equation (4). Whereas the heat transfer in porous media (e.g. ground layers with groundwater flow) is described by the following equations:

$$(\rho c_p)_{\text{eq}}\frac{\partial T}{\partial t} + \rho_{\text{gw}} c_{p,\text{gw}} u\cdot\nabla T = \nabla\cdot(\lambda_{\text{eq}}\nabla T) \quad (5)$$

$$(\rho c_p)_{\text{eq}} = \theta_{\text{p}}\rho_{\text{g}} c_{p,\text{g}} + (1-\theta_{\text{p}})\rho_{\text{gw}} c_{p,\text{gw}} \quad (6)$$

$$\lambda_{\text{eq}} = \theta_{\text{p}}\lambda_{\text{g}} + (1-\theta_{\text{p}})\lambda_{\text{gw}} \quad (7)$$

In the above equations, $(\rho c_p)_{\text{eq}}$ and λ_{eq} are the equivalent volumetric heat capacity and equivalent thermal conductivity of the porous medium in which the groundwater flows. Whereas ρ_{gw}, $c_{p,\text{gw}}$ and λ_{gw} are the density, specific heat capacity and thermal conductivity of groundwater.

In this work, the groundwater flow in a porous media is described by Darcy's law that is given as below:

$$\frac{\partial}{\partial t}(\rho\epsilon_{\text{p}}) + \nabla\cdot(\rho u) = G_{\text{m}} \quad (8)$$

$$u = -\frac{k}{\mu}\nabla p \quad (9)$$

In the above equations, θ_{p} and ϵ_{p} are the volume fraction and the porosity, respectively, and their overall sum yield a unity; k is the permeability and u is the groundwater velocity. Whilst p is the hydrodynamic pressure. G_{m} stands for the mass source, which is set to zero.

Boundary conditions

In this research, the focus is to develop STES models that are reliable and computationally fast enough to give insights on the design of STES. Therefore, system simulations are not considered at this stage and this means no DH system is actually modeled. However, the DH operation profiles (temperature and flowrate) are of importance for the operation of STES system, especially for the charging/discharging modes. Therefore, a simplified standard DH temperature profile is introduced in the model, where the DH supply temperature is set to 90 °C and the return temperature is given as 60 °C. Figure 2 and Figure 3 show the simplified periodic operating conditions for a TES. Further, Figure 4 shows the simplified scheme of charging/discharging processes used in STES modelling.

Additionally, the dimensions for both storage options (tank and pit) are shown in Table 1. While the different thermo-physical properties and the heat transfer coefficients used for the materials in the modeling of the STES are reported in Table 2. Moreover, Table 3 documents the values of the different properties used for the groundwater flow.

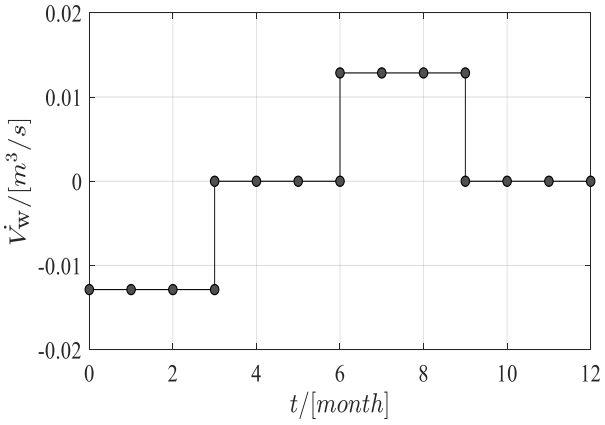

Figure 2: Water volumetric flowrate as a periodic function of the time for a TES with a volume of 100000 m³.

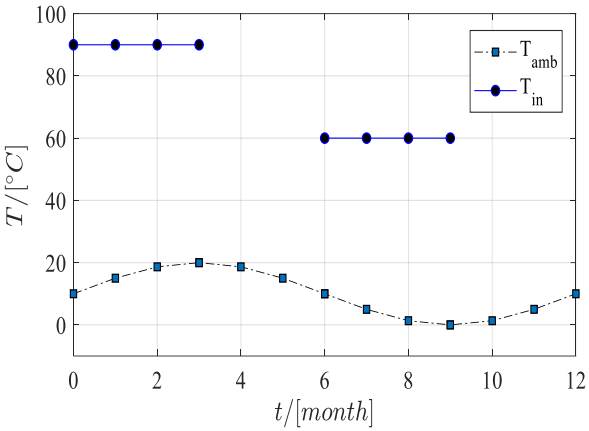

Figure 3: Flow temperature as a periodic function of the time and ambient temperature as a sinus function with an average of 10°C.

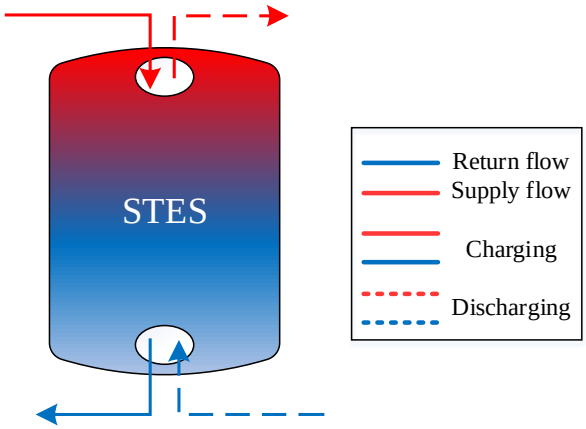

Figure 4: Representation of the simplified scheme used for charging side (continuous) and discharging side (dashed) in STES modelling.

Table 1: Dimensions of the TES for two options (tank and pit)

Parameter	**Tank**	**Pit**
Height, H	50 m	50 m
Base diameter, d_b	50.5 m	20 m
Top surface diameter, d_a	50.5 m	75.7 m
Slope angle, α	90°	60.9°
Volume, V	100 000 m^3	100 000 m^3

Table 2: Thermo-physical properties of the materials and heat transfer coefficients (HTC) of the different components in TES

Parameter	**Value**
Water thermal conductivity, λ_w	0.6 W/(m.K)
Water density, ρ	1000 kg/m^3
Water specific heat capacity, c_p	4200 J/(kg.K)
Overall HTC of the cover, U_{cover}	0.1 W/(m^2.K)
Overall HTC of the wall, U_{wall}	0.3 W/(m^2.K)
Overall HTC of the bottom, U_{bottom}	0.3 W/(m^2.K)
Ground thermal conductivity, λ_g	1.5 W/(m.K)
Ground specific heat capacity, $c_{p,g}$	880 J/(kg.K)
Ground density, ρ_g	1000 kg/m^3

Table 3: Exemplary groundwater properties set in the 3-D model

Parameter	**Value**
Volume fraction, θ_p	0.7
Porosity, ϵ_p	0.3
Permeability, k	10^{-7} m^2
Dynamic viscosity, μ	$72.5 \cdot 10^{-5}$ Pa.s
Groundwater inflow velocity, u_0	0.00002 m/s

Results and Discussion

The time-dependent problem described above is simulated using the tool COMSOL Multiphysics. The maximum time step corresponds to 1 day. Simulations with lower time steps showed more computational efforts with no more significant changes on results.

In order to reduce the impact of the initial conditions on the results, the simulation time span set to either 3 years or 10 years.

Water temperature

Temperature distribution of water along z-axis is investigated for both options (tank and pit). Figure 5 and Figure 6 display the simulated temperature of water in STES for different time steps. The simulation starts with a uniform temperature profile for the three cases (charging, standby and discharging). The storage is cooled down with an average ambient air temperature of 10°C from the top, whereas the ground temperature has an impact on the lateral and bottom areas of the storage. It can be observed that thermal stratification gradually takes place in the storage. Consequently, the thermo-hydraulic behavior of water is correctly implemented and the model qualitatively provides correct results.

Performance evaluation

A number of simulations, each with 10 years, were carried out to evaluate the performance of both STES types (tank and pit).

In Figure 7, however, it is seen that the pit TES has lower energy content compared to the energy content of the tank. This is attributed to the heat transfer rates from the storage to the ground (i.e. thermal losses). Moreover, the storage temperature contributes significantly to this variation since the pit has water stored at ~60°C (Figure 6), whilst the tank stores water at a minimum temperature of ~82°C (Figure 5). Later, this has a significant influence on the discharge phase as shown in Figure 5 and Figure 6. In fact, the pit discharges faster compared to the tank because the tank-discharged energy is higher than that of the pit as proven in Figure 9.

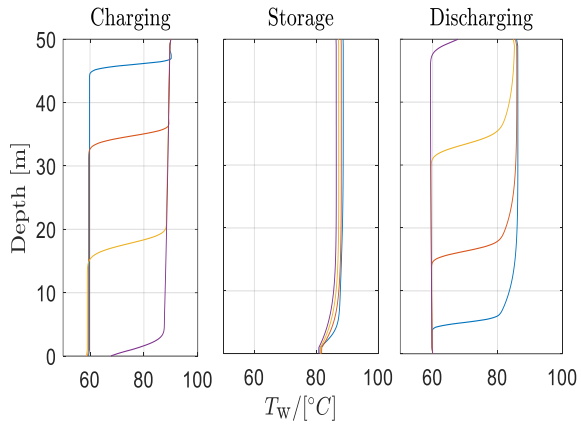

Figure 5: Tank water temperature along z-axis for the three phases (charging, storage and discharging) at different time steps (Charging: 10, 30, 60 and 90 days; Storage: 100, 120, 150 and 180 days; Discharging: 190, 210, 240 and 270 days).

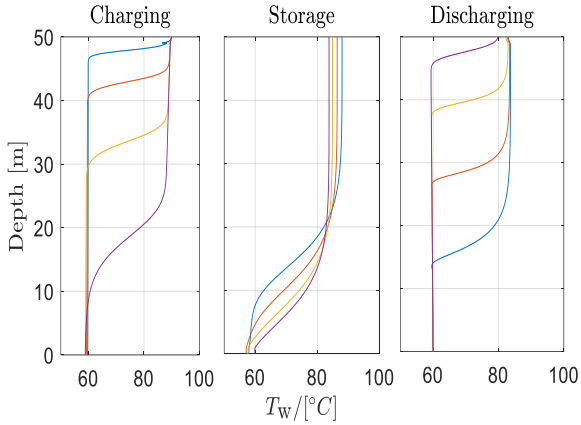

Figure 6: Pit water temperature in the pit along z-axis for the three phases (charging, storage and discharging) at different time steps (Charging: 10, 30, 60 and 90 days; Storage: 100, 120, 150 and 180 days; Discharging: 190, 210, 240 and 270 days).

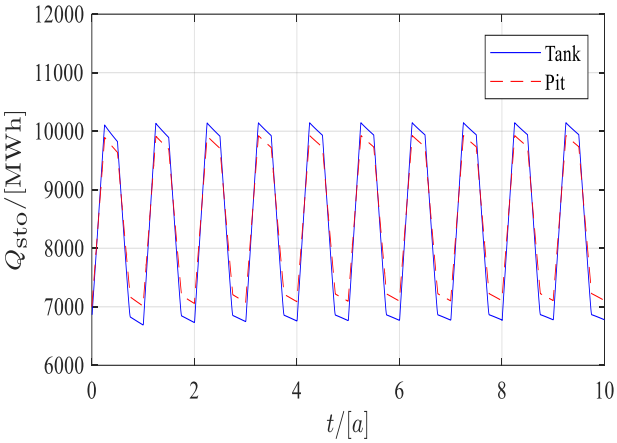

Figure 7: Energy content of the tank (blue) and pit (red) during the ten years of investigation.

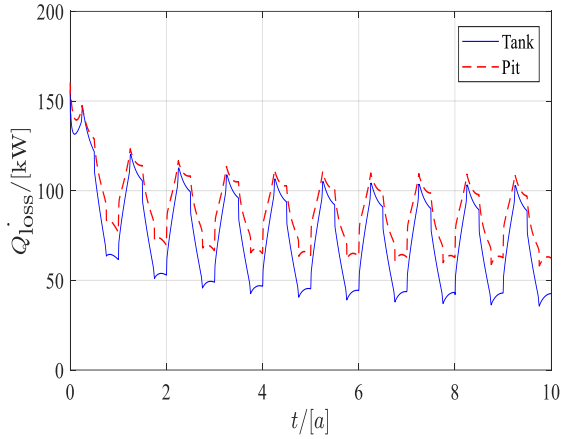

Figure 8: Thermal losses from the tank (blue) and the pit (red) during the 10 years of investigation.

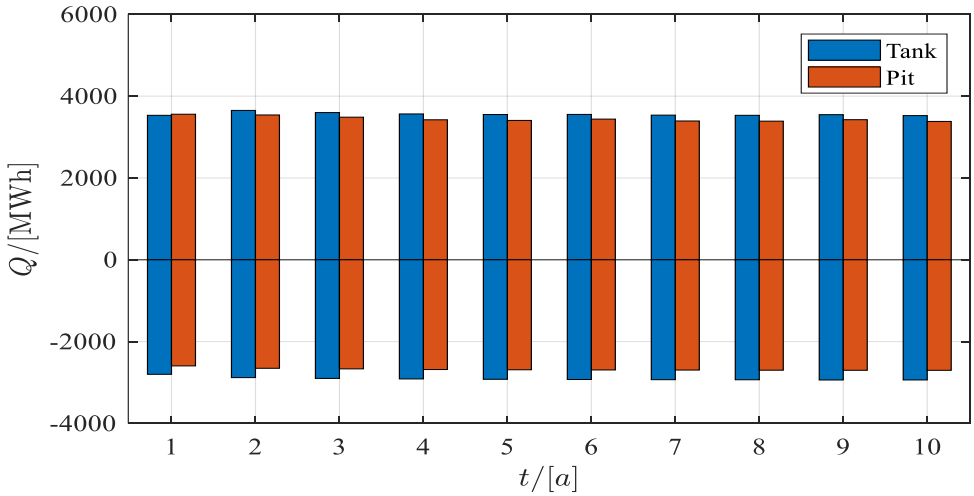

Figure 9: Annual charged (positive) and discharged (negative) energy from tank (blue bars) and pit (red bars) in case of insulation. Higher discharge and charge rates are observed for the tank.

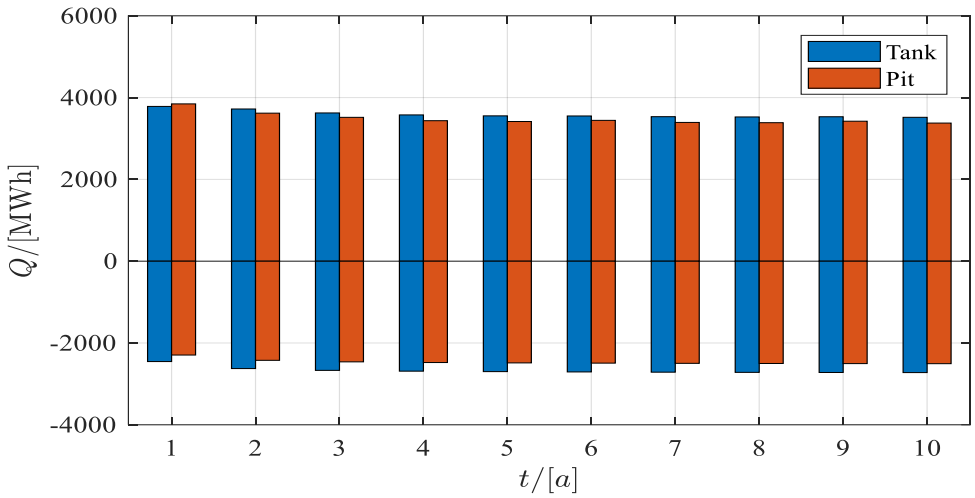

Figure 10: Annual charged (positive) and discharged (negative) energy from tank (blue bars) and pit (red bars) in case no insulation. Higher discharge and charge rates are observed for the tank.

In Figure 8, it is shown that thermal losses tend to decrease continuously and, in return, this triggers the energy content to rise. In fact, this pattern is attributed to the surroundings (i.e. ground/soil) temperature and ground thermal conductivity. The surroundings temperature is presumed at 10°C as an initial value and, therefore, a heat transfer process is initiated between the storage and the surroundings causing an increase in surroundings temperature over time until it reaches a steady pattern. This is seen from the third year and up.

Moreover, it is remarkably shown that pit has higher thermal losses compared to the tank and, consequently, less energy content. The main reason behind the higher losses is the pit has bigger top surface area than the tank, which induces a drop in the water temperature at the top as proven by Figure 5 and Figure 6 and, additionally, less discharged energy than that of the tank as shown in Figure 9.

Moreover, another case was inspected for both storage options (tank and pit) with same dimensions given in Table 1; this case involves no insulation used over the storage sidewalls and bottom. Whilst other boundary conditions shown in Table 2 remained the same. Figure 10 depicts that the tank-discharged energy is also higher in this case. Nevertheless, it is observed that tank-discharged energy in case of no insulation is less by an average of 7.3 % (corresponding to appx. 214 MWh) compared to the case of when insulation is used for the year 10 of the investigation period.

To capture the storage performance, it is crucial to evaluate the thermal efficiency of the storage and then compare the values for both options (tank and pit) in both cases (with and without insulation). The storage efficiency obeys the following equation:

$$\eta_{\text{sto}} = 1 - \frac{\sum_{i=1}^{t} Q_{\text{loss}}}{Q_{\text{sto}}} \qquad (10)$$

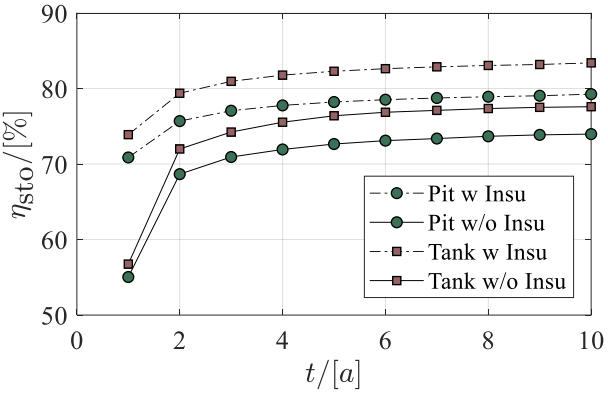

Figure 11: Storage efficiency calculated from the thermal losses and storage energy content during the 10 years of simulation.

In equation (10), the thermal losses are calculated a year-round, which means that also the thermal losses during the idle phase (the phase between the discharging and charging) are included. In fact, it also plays a role in the energy balance of the storage. The thermal losses are calculated step-by-step and integrated all over the year. Figure 11 shows the storage efficiency plotted for each year of investigation for two cases (with and without insulation). In both cases, it is observed that the tank outperforms the pit due to the difference in thermal losses (see Figure 8). From Figure 11, it can be observed that the efficiency broadly increases with an asymptotic trend. Yet, starting from the 5th year the efficiency slightly rises. This draws attention to an interesting argument that under the given boundary conditions, material properties for the storage and the ground, the storage reaches a steady operation after about 5 years. For other boundary conditions, however, this might differ depending on, for example not limited, the thermal resistance of insulation. Moreover, it is also noticed that tank efficiency in case no insulation approaches the pit efficiency when insulation is used. Therefore, a techno-economic analysis is required to evaluate the options more comprehensively.

Furthermore, the low efficiency over the course of the first 5 years (1st to 5th year) is attributed to the ground thermal properties. In fact, thermal losses are strongly driven by the ground temperature and the ground thermal conductivity. The ground temperature increases producing a lower temperature difference between the storage and the ground and, therefore, less thermal losses and higher efficiency.

Cut-off walls as a groundwater flow controller

Under favorable hydro- geological conditions (e.g. no groundwater), it is held that the storage has better performance because the existence of groundwater might lead to an increase in the effective thermal conductivity of the ground and, therefore, higher thermal losses. However, it is difficult to install the storage in a place ensuring no groundwater flows. Figure 12 highlights the impact of groundwater flow. Thereby bringing higher thermal losses by around 15 % compared to the case when no groundwater exists. Consequently, a notable decrease in the efficiency will likely take place. One the other hand, hydro- geologically speaking, there exist some national and/or regional standards that prevent the groundwater temperature from increasing beyond 20°C to 25°C in some countries. Therefore, it is important to count on a method that is capable to exclude the groundwater flow from the storage structure whereby a crucial aspect is to reduce the thermal losses from the storage and, consequently, it provides better performance.

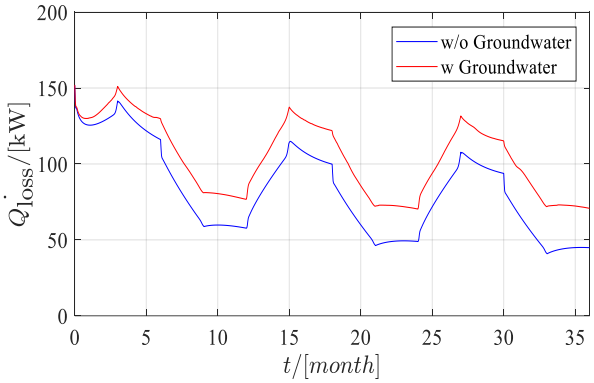

Figure 12: Comparison of thermal losses form a tank storage for two cases: one without groundwater flow (blue) and another with groundwater flow (red).

Different techniques are used during excavation phase to control and/or restrict the groundwater flow. These methods are typically classified into pumping- or excluding-based. In this work, the exclusion method is chosen whereby a groundwater flow is reduced or avoided nearby the storage structure by installing impermeable vertical physical walls forming the so-called “cut-off walls”. Cut-off walls are underground barriers at different heights to preserve the quality of groundwater and to reduce the thermal losses. They are often serving as practical engineering solutions.

In this work, the cut-off wall was employed to reduce the influence of groundwater. Herein, the main characteristic investigated was the distance from the storage envelope to the cut-off wall. Thus, a parametric study was carried out to determine the distance impact on storage thermal losses, whereby the distance ranged between 1 m and 10 m.

Figure 13 compares the thermal losses for one annual operation cycle in the tank with a given volume in two cases: with and without groundwater flow. Moreover, it indicates also the impact of a cut-off wall on the thermal losses. By presenting the breakdown, it is noticed that the increase in thermal losses occur in side part because the groundwater flow has a direct contact with the sidewalls of the tank and, therefore, the change in top and bottom thermal losses are negligible. To reduce the impact of groundwater, cut-off walls are introduced. From Figure 13, it is observed the farther the cut-off wall, the less the influence is and, thereby, less thermal losses compared to the case with groundwater flow and no cut-off wall.

Conclusion

Large-scale seasonal thermal energy storage represents an intrinsic element in SDH applications since it provides a considerable robustness to the overall system. Numerical simulations for large-scale STES systems arise as an alternative to real on site experiments. In this study, a 2-D numerical modeling approach was presented for axisymmetric geometries (cylindrical tank and conical pit). The approach was tested and, then, a comparison driven by temperature profiles and storage performance between both storage options was shown. The results indicate that under the given boundary conditions (see Table 1 and Table 2), the tank outperforms the pit by approximately 4 % more in context of efficiency. The same applies when no insulation was used. Further, it is depicted that the tank without insulation has approximately similar efficiency as that of the pit with insulation after the ground pre-heating period. Also, the results depicted that the storage reaches stable operation only after 5 years for the given storage volume and boundary conditions. Yet, this time slot of 5 years can vary depending on many players (e.g. insulation thickness, ground thermal conductivity).

Next, the work underlined the role of hydro- geological conditions on storage performance by comparing a favorable hydro- geological condition (no groundwater flow) against an extreme case (high groundwater streamflow). Thus, a 3-D numerical model for the tank was developed. The outcomes revealed a remarkable increase in the thermal losses when groundwater exists. In fact, when no groundwater flows, then only conductive heat transfer from the storage to the ground occurs. On the other hand, another contribution is added, which is the convective part, if the groundwater flow was included. Consequently, cut-off walls enclosing the storage were introduced to reduce the groundwater impact. Different distances from the storage were investigated. It is concluded the farther the wall, the better the performance is. However, the cost of installing such structures also play a role in determining the optimum distance. Moreover, future work will focus on the validation of the models against measured data from real storage plants.

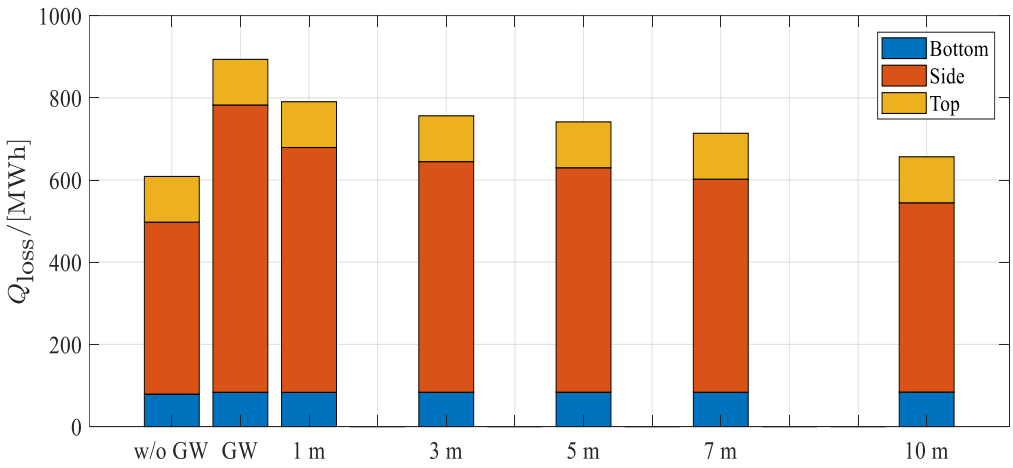

Figure 13: Breakdown of the thermal losses for the tank with and without groundwater flow.

Acknowledgement

This project is financed by the Austrian "Klima- und Energiefonds" and performed in the frame of the program "Energieforschung". It is part of the Austrian flagship research project "Giga-Scale Thermal Energy Storage for Renewable Districts" (giga_TES, Project Nr.: 860949). Therefore, the authors acknowledge the financial support.

Nomenclature

Symbol	Description	Unit
A	Area	m^2
c_p	Specific heat cpacity	J/(kg.K)
G_m	Mass source	kg/(m^2.s)
k	Permeability	m^2
$\dot{m}$	Mass flowrate	kg/s
p	Pressure	Pa
$\dot{q}$	Heat flux	W/m^2
Q	Heat (i.e. thermal energy)	J
$\dot{Q}$	Heat flowrate	W
T	Temperature	K
t	Time step	s
U	Thermal transmittance	W/(m^2.K)
u	Velocity	m/s
z	Vertical axis inside the tank	m
ϵ	Porosity	-
η	Efficiency	%
Θ	Volume fraction	-
λ	Thermal conductivity	W/(m.K)
μ	Dynamic viscosity	Pa.s
ρ	Density	kg/m^3

References

Allegrini, J. et al. (2015). A review of modelling approaches and tools for the simulation of district-scale energy systems. *Renewable and Sustainable Energy Reviews, 52*, 1391-1404.

Chang, C. et al. (2017). Influences of the key characteristic parameters on the thermal performance of a water pit seasonal thermal storage. *Energy Procedia, 142*, 495-500. doi:10.1016/j.egypro.2017.12.077

Dahash, A. et al. (2018). Detailed Axial Symmetrical Model of Large-Scale Underground Thermal Energy Storage. *Proceedings of the 2018 COMSOL Conference.* Lausanne (Switzerland), 22-24 October 2018.

Dahash, A. et al. (2019). A comparative study of two simulation tools for the technical feasibility in terms of modeling district heating systems: An optimization case study. *Simulation Modelling Practice and Theory, 91*, 48-68.

Dahash, A. et al. (2019). Advances in Seasonal Thermal Energy Storage for Solar District Heating Applications: A Critical Review on Large-Scale Hot-Water Tank and Pit Thermal Energy Storage Systems. *Applied Energy, 239*, 296-315. doi:10.1016/j.apenergy.2019.01.189

Mazhar, A. R. et al. (2018). A state of art review on the district heating systems. *Renewable and Sustainable Energy Reviews, 96*, 420-439.

Ochs, F. (2009). *Modelling Large-Scale Thermal Energy Stores, Ph.D. Dissertation.* Stuttgart: Shaker Verlag.

Ochs, F. (2014). Large-Scale Thermal Energy Stores in District Heating Systems – Simulation Based Optimization. *Proceedings of EuroSun 2014: International Conference on Solar Energy and Buildings.* Aix-les-Bains (France), 16-19 September 2014.

Panthalookaran, V. et al. (2008). Calibrated models for simulation of stratified hot water heat stores. *International Journal of Energy Research, 32*(7).

Panthalookaran, V. et al. (2011). The Effects of Boundary Design on the Efficiency of Large-Scale Hot Water Heat Stores. *Journal of Solar Energy Engineering, 133*(4).

Schmidt, T. and Sørensen, P. A. (2018). Monitoring Results from Large Scale Heat Storages for District Heating in Denmark. *EnergSTOCK2018: 14th International Conference on Energy Storage.* Adana (Turkey), 25-28 April 2018.